Atomic structure of hot compressed borosilicate glasses

Ding, Linfeng; Lee, Kuo-Hao; Zhao, Tongyao; Yang, Yongjian; Bockowski, Michal; Ziebarth, Benedikt; Wang, Qingwei; Ren, Jinjun; Smedskjær, Morten Mattrup; Mauro, John C.

Published in:
Journal of the American Ceramic Society

DOI (link to publication from Publisher):
10.1111/jace.17377

Publication date:
2020

Document Version
Accepted author manuscript, peer reviewed version

DR LINFENG DING (Orcid ID : 0000-0002-1447-5598)
DR MORTEN SMEDSKJAER (Orcid ID : 0000-0003-0476-2021)
DR JOHN C. MAURO (Orcid ID : 0000-0002-4319-3530)

Article type : Article

Atomic Structure of Hot Compressed Borosilicate Glasses

Linfeng Ding[1,2], Kuo-Hao Lee[2], Tongyao Zhao[3], Yongjian Yang[2], Michal Bockowski[4], Benedikt Ziebarth[5], Qingwei Wang[1]*, Jinjun Ren[3], Morten M. Smedskjaer[6] and John C. Mauro[2]*

[1]State Key Laboratory for Modification of Chemical Fibers and Polymer Materials, Donghua University, Shanghai 201620, China

[2]Department of Materials Science and Engineering, The Pennsylvania State University, University Park, PA 16802, USA

[3]Key Laboratory of Materials for High Power Laser, Shanghai Institute of Optics and Fine Mechanics, Chinese Academy of Sciences, Shanghai 201800, China

[4]Institute of High-Pressure Physics, Polish Academy of Sciences, Warsaw, Poland

[5]Schott AG, Corporate Research & Development, Mainz 55122, Germany

[6]Department of Chemistry and Bioscience, Aalborg University, Aalborg DK-9220, Denmark

*Corresponding author: jcm426@psu.edu, wqwq888@dhu.edu.cn

Abstract

Borosilicate glasses have been in widespread use for over a century; however, a detailed understanding of the structural response to densification is still lacking. In this work, two commercial borosilicate glasses, viz., SCHOTT N-BK7® (N-BK7) and Borofloat33® (Boro33), are hot compressed up to 2 GPa with nitrogen gas, and the structural response to this densification is explored via ^{11}B solid-state nuclear magnetic resonance (NMR) spectroscopy and classical molecular dynamics (MD) simulations. The molar volume (V_m) of N-BK7 and Boro33 decreases ~5% and ~10%, respectively, as a result of hot compression at 2 GPa. The NMR results demonstrate the presence of three different types of fourfold coordinated boron species ($B^{[4]}$), which are confirmed in MD simulations to be $B_1^{[4]}$(0B,4Si$^{[4]}$), $B_2^{[4]}$(1B$^{[3]}$,3Si$^{[4]}$) and $B_3^{[4]}$(1B$^{[4]}$,3Si$^{[4]}$) (where subscripts represent different $B^{[4]}$ types and brackets indicate the next nearest neighbors (NNN)). The NMR results also show that the fraction of $B^{[4]}$ increases by ~13% in N-BK7 glass upon hot compression at 2 GPa via the trigonal boron to tetrahedral boron ($B^{[3]}$ to $B^{[4]}$) conversion, while the fraction of $B^{[4]}$ in Boro33 glass only increases by ~2% at the same pressure, despite the fact that the V_m decrease in N-BK7 is double that of Boro33. The MD simulations capture the experimental trends in $B^{[4]}$ populations, despite an underestimation of the $B^{[4]}$ increase of N-BK7 (only ~6 %) at 2 GPa. Moreover, the MD simulations suggest that the V_m reduction is a linear function of bond angle change and the fraction of Si-O-Si and $B^{[4]}$-O-Si. The modifiers and boron coordination conversion also influence the volume densification of borosilicate glasses by increasing the difficulty of bond bending, decreasing the bond lengths, and increasing the population of $B^{[4]}$-O-Si linkages. Lastly, the $B^{[4]}$ to $B^{[4]}$ conversion, i.e., $B_2^{[4]}$(1B$^{[3]}$,3Si$^{[4]}$) and $B_3^{[4]}$(1B$^{[4]}$,3Si$^{[4]}$) to $B_1^{[4]}$(0B,4Si$^{[4]}$), is observed in hot compressed N-BK7 and Boro33 from NMR and qualitatively confirmed in MD.

Keywords: borosilicate glass; densification; nuclear magnetic resonance spectroscopy; structure; molecular dynamics simulations

1. Introduction

Borosilicate glasses are widely applied in industry and daily life due to their excellent performance in various environments, e.g., as substrate or cover glass for display panels and personal electronic devices, optical glass for microscopes, container glass for kitchen and laboratories, glass fiber for composites and insulation, etc.[1] Despite its widespread use for over a century, understanding of the atomic scale origins of the structure-property response in densified glass is still lacking.[2] Such understanding is crucial for developing new glass products with improved performance and optimized mechanical properties. For example, pressure provides an additional degree of freedom to precisely control the interatomic structure of glass as well as induce permanent property changes upon hot-compression treatment.[3] Moreover, the structural evolution of B_2O_3 in silicate-based magmatic melts, particularly under high pressure, is still an unsolved fundamental question for the dynamics of magmatic melts in the earth.[4]

One of the key structural features for borosilicate glass is the conversion of trigonal boron ($^{[3]}$B) to tetrahedral boron ($^{[4]}$B), which can be observed upon variation of composition[5], temperature[6], and pressure[7, 8, 9]. This boron coordination change can be induced near the glass transition range and elevated pressure (higher than several hundred megapascals), which has a great impact on the structure and properties of borosilicate glass[10, 11]. For example, Sen et al.[6] reported the temperature dependence of boron coordination change as the most important source contributing to configurational entropy, which directly links to structural changes and viscous flow. Wondraczek et al.[12] described an equivalence relation between temperature and pressure effects on $^{[4]}$B fraction and molar volume, that is, 400 MPa and 4 K/min gives an equivalent effect as 0.1 MPa and 10^{-4} K/min. Moreover, the $^{[3]}$B to $^{[4]}$B conversion has been found to also take place at room temperature under high pressure (e.g., 2 GPa)[7].

Among all the studies on hot-compression-induced densification of borosilicate glasses, various studies reported a significant $^{[3]}$B to $^{[4]}$B conversion with increasing pressure (several hundred megapascals to 2 GPa). [8, 9, 10, 13, 14] However, an early nuclear magnetic resonance (NMR) study[14] on several potassium borate glasses reported no detectable $^{[3]}$B to $^{[4]}$B conversion at 2.5 GPa. The puzzle of the origin of $^{[3]}$B to $^{[4]}$B conversion under high pressure is thus still missing several pieces.

In this work, we choose two commercial borosilicate glasses, namely SCHOTT N-BK7® and SCHOTT Borofloat33®. Both glasses have a similar concentration of B_2O_3, similar glass transition temperature ($T_{g,vis}$) and Poisson's ratio, but quite different density and mechanical properties. The atomic origin of these two widely used borosilicate glasses under high pressure, especially the role of boron, is still an area of active research. Fortunately, ^{11}B NMR has long been applied to study the short-range structure of borosilicate glass and provide precise information on boron species.[5] Also, recently developed B-O interatomic potentials[15, 16, 17, 18] for classical molecular dynamics (MD) simulations have been reported which can reliably reproduce the B[4] fraction of borosilicate glasses. Thus, we evaluate the pressure-structure-property relationships by applying a combination of solid-state NMR spectroscopy and MD simulations to explore the atomic origin of volume densification of borosilicate glass.

2. Methods

2.1 Experimental methods

The compositions and basic properties of SCHOTT N-BK7® (ID: N-BK7) and SCHOTT Borofloat33® (ID: Boro33) are reported in Table 1. All the cylindrical samples were provided by SCHOTT AG with a size of 7 mm (diameters) × 8 mm (lengths) and mirror-polished surfaces.

Two glass samples (N-BK7 and Boro33) were placed inside a graphite furnace in a vertical stack, which was separated by a 2 mm alumina disk, and subjected to an isostatic high-pressure treatment by applying a nitrogen medium high-pressure apparatus. All the experiments were conducted at 560 ℃-700 ℃ under 1 GPa or 2 GPa for 0.5 h to evaluate the influence from both pressures. Followed by a controlled cooling down to room temperature at a constant rate of 2 K/min. Finally, the system was decompressed at a rate of 30 MPa/min to ambient pressure.

After the hot compression treatments[19], the density of samples was measured by Archimedes principle in demineralized water. Each density measurement was repeated five times to obtain a standard deviation as the measurement uncertainty. Afterwards, the samples were crushed into fine powders for the solid-state ^{11}B NMR spectroscopy measurements.

^{11}B solid-state NMR experiments were carried out on a Bruker Avance III HD 500 M spectrometer (11.7 T). The resonance frequency is 160.5 MHz. All the spectra were recorded using a

4-mm Bruker magic angle spinning (MAS) probe. ^{11}B MAS spectra were obtained at a spinning speed of 10 kHz. The pulse length is 0.8 μs (15° liquid angle) with a recycle delay of 32 s. Chemical shifts were referenced to 1 M H_3BO_3 solution.

2.2 Molecular dynamics simulations

Precise prediction of structure-property relations in borosilicate glass at the atomic scale is a very challenging task due to the lack of reliable interatomic potentials for MD simulations[20]. Recently, Fortino, et al.[20] tested three B-O interatomic potential models and drew the conclusion that the potentials proposed by Du[17] and Bauchy[21] can both reliably reproduce the $B^{[4]}$ fraction of borosilicate glasses. Moreover, MD simulation results from Lee et al.[22] suggested that Du's potential more accurately predicts the $B^{[4]}$ fraction for N-BK7 glass, while Bauchy's potential better predicts the $B^{[4]}$ fraction for Boro33 glass compared to the neutron diffraction[23] measurements. Therefore, following Lee's work[22], Du's potential was applied for modeling the N-BK7 glass by introducing the $B^{[4]}$ fraction predicted by DBX model[24] (1 atm) as an input parameter, and Bauchy's potential was selected for the Boro33 glass.

Both Du's and Bauchy's potentials adopt the same form of a short-range Buckingham term combined with a long-range Coulomb term, which can be expressed as:

$$U(r_{ij}) = {z_i z_j e^2}/{r_{ij}} + A_{ij} e^{{-r_{ij}}/{\rho_{ij}}} - {C_{ij}}/{r_{ij}^6} \quad (1)$$

where z_i and z_j are the reduced (partial) charges of atom i and atom j, r_{ij} is the interatomic distance between atom i and atom j, and A_{ij}, C_{ij}, and ρ_{ij} are the fitting constants. A splice correction is added to prevent the problem caused by the Buckingham potential at low r_{ij} region in Du's potential, which is described as:

$$U'(r_{ij}) = {B_{ij}}/{r_{ij}^n} + D_{ij} {r_{ij}}^2 \quad (2)$$

in which B_{ij}, D_{ij}, and n are fitting parameters.

LAMMPS (Large-scale Atomic/Molecular Massively Parallel Simulator)[25] software was employed for the MD simulations. A cutoff of 11 Å was applied for both the short-range and

Coulombic interactions. The Particle-Particle Particle-Mesh (PPPM) algorithm was used for calculating the long-range forces with an accuracy of 10^{-5}. Periodic boundary conditions were applied in all directions in each of the simulations.

We note that both the Du and Bauchy potentials are not parameterized for simulating the melt-quench process under high-pressure conditions. Nevertheless, following an approach tested by Bauchy[26], glass samples with different densities were run in the canonical ensemble (NVT) to account for the pressure effect in MD simulations. Five parallel initial configurations for each type of glass were randomly generated with 3073 atoms created in a cubic simulation box. The box size was calculated based on the densities of the samples annealed at 1 atm and hot compressed at 1 GPa and 2 GPa. All the samples were melted at 6000 K for 100 picoseconds (ps) and at 5000 K for 1000 ps to eliminate the memory of the initial configuration, followed by a quench from 5000 K to 300 K at the rate of 5 K/ps. A subsequent relaxation was conducted at 300 K using the NVT ensemble for 60 ps, and a final statistical averaging was run as NVT for 60 ps. The above procedure follows the previous work of Deng et al.[17] by switching the NPT ensemble during relaxation at 300 K to NVT ensemble. One femtosecond (fs) was used as the integration timestep throughout all the simulations. A computed pressure of 0.2 GPa was found in N-BK7 glass (using Du's potential) after the statistical averaging at 300 K and one of -1.8 GPa is found in Boro33 glass (Bauchy's potential). The pressure at room temperature density is due to the choice of potential, but it has been confirmed that the pressure dependence of structural changes can be calculated[26].

3. Results

3.1 NMR

The ^{11}B MAS NMR spectra of N-BK7 glass and Boro33 glass at various pressure and temperature conditions are shown in Figure 1. All the NMR spectra have been area normalized by applying the trapezoidal[27] numerical integration function in Matlab and fitting by Dmfit[28] to reproduce the line shapes of the different boron species. Blue dashed curves in Figure 1 are the deconvolutions and full fits of the NMR spectra for samples prepared at 1 atm. Based on numerous studies[5, 8, 14, 29, 30, 31, 32, 33] on borosilicate glasses, the blue dashed curves at the sites of 17.3 ppm, 13.3 ppm, -0.2 ppm, and 2 ppm can be assigned to trigonal boron in ring units ($B^{[3]}$ ring), trigonal boron

not in rings ($B^{[3]}$ nonring), tetrahedral boron connected to 1 $B^{[3]}$ and 3 $Si^{[4]}$ ($B_2^{[4]}$(1$B^{[3]}$,3$Si^{[4]}$)) and tetrahedral boron connected to 4 $Si^{[4]}$ ($B_1^{[4]}$(0B,4$Si^{[4]}$), $B^{[4]}$ type 1), respectively. Interestingly, a site at -1.3 ppm corresponding to $B_3^{[4]}$ ($B^{[4]}$ type 3) is also observed in NBK7, which, to our best knowledge, has not been reported in the literature.

The boron speciation results from the NMR analysis are summarized in Table 2. First, the fractions of tetrahedral boron to total boron (N_4 or $B_{total}^{[4]}$) of as-prepared (1atm-560 ℃/4 h) samples are 86 ± 2 % for N-BK7 and 21 ± 2 % for Boro33, which are close to the previous values from neutron diffraction[23] measurements (91 % and 23 %) and MD simulations[22] (90 ± 1 % and 20 ± 2 %). Second, $B^{[3]}$ converts to $B^{[4]}$ with increasing pressure in N-BK7 glass, while both $B^{[3]}$ and $B^{[4]}$ fractions show only minor changes as a function of pressure in Boro33 glass. The pressure-induced $B^{[3]}$ change can be seen in the inset figure of Figure 1(a). Specifically, the molar volume decreased ~5 % at 2 GPa accompanied by a $B^{[4]}$ increase of ~13 % for N-BK7 glass. On the other hand, a molar volume decrease of ~10 % while $B^{[4]}$ increased only less than 2 % (within the error bar) is found for Boro33, as illustrated in Figure 2. Lastly, a $B^{[4]}$ to $B^{[4]}$ conversion is detected in both N-BK7 and Boro33 glass, during which the $B^{[4]}$ ratios ($\frac{B_1^{[4]}}{B_3^{[4]}}$ for N-BK7 glass and $\frac{B_1^{[4]}}{B_2^{[4]}}$ for Boro33 glass) are increasing as a function of pressure, and simultaneously, $B_3^{[4]}$(-1.3 ppm) and $B_2^{[4]}$(1$B^{[3]}$,3$Si^{[4]}$) are gradually transformed to $B_1^{[4]}$(0B,4$Si^{[4]}$) with increasing pressure. This $B^{[4]}$ to $B^{[4]}$ conversion phenomenon is even more distinct in Figure 1(b), in which two main peaks are observed in the 1 GPa samples and the $B_1^{[4]}$ peaks are significantly enhanced from 1 atm to 2 GPa. Moreover, the isothermal holding temperature will also have a significant influence on the $B^{[4]}$ to $B^{[4]}$ conversion. The $B^{[4]}$ ratios increase with an increase in temperature (580 ℃, 600 ℃, and 700 ℃) for both N-BK7 and Boro33 glasses compressed at 2 GPa, while all the N-BK7 samples compressed at 1 GPa reached similar $\frac{B_1^{[4]}}{B_3^{[4]}}$ value with the increase of temperature (560 ℃, 580 ℃, and 600 ℃). This indicates an equilibrium state of $B^{[4]}$ as the Boro33 samples compressed at 1 GPa only have a slight increase in $\frac{B_1^{[4]}}{B_2^{[4]}}$. The pressure and temperature dependence of $B^{[4]}$ to $B^{[4]}$ conversion of Boro33 glass can be seen in Figure 1(b).

3.2 MD simulations

The peak assignment for $B^{[4]}$ is primarily based on the results from ^{11}B and ^{17}O NMR spectroscopic studies.[5] In this study, we performed MD simulations to directly check the boron species and explore the atomic origin of the volume densification in the borosilicate glasses. The V_m of the MD samples was set to be equal to the experimental values: N-BK7: V_m=7.86 cm^3/mol (~1 atm), V_m=7.66 cm^3/mol (~1 GPa), and V_m=7.46 cm^3/mol (~2 GPa); Boro33: V_m=8.64 cm^3/mol (~1 atm), V_m=8.18 cm^3/mol (~1 GPa), and V_m=7.80 cm^3/mol (~2 GPa). The N_4 results in Table 2, which is presented as $B^{[4]}_{MD}$, exhibit a similar overall trend as a function of pressure compared to NMR experiments. N_4 of N-BK7 increases from 89% to 95% (~6%) at 2 GPa, which is less significant than the increase in N_4 determined from NMR from 86% to 99% (~13%). We note that only one N_4 input (predicted from DBX model[24]) is applied in Du's potential for all the other MD simulations on N-BK7 glass. Moreover, the N_4 change in Boro33 is not significant compared to the uncertainty of the simulations (~2%) which is consistent with the result from NMR (~2%).

To explore the chemical environment around $B^{[4]}$, the fraction next nearest neighbors (NNN) of $B^{[4]}$ in N-BK7 and Boro33 glasses are presented in Figure 3. The NNN calculations indicate that $B^{[4]}(0B,4Si^{[4]})$ is the most frequent species in both N-BK7 and Boro33, while the second most frequent one in N-BK7 is $B^{[4]}(1B^{[4]},3Si^{[4]})$ and that of Boro33 is $B^{[4]}(1B^{[3]},3Si^{[4]})$. Although the $B^{[4]}$-O-$B^{[4]}$ linkage has previously been reported as energetically unfavorable[14], as interpreted based on the results from $Al^{[4]}$-O-$Al^{[4]}$ linkages in aluminosilicates[34, 35], recent studies[36, 37] based on double quantum ^{11}B NMR and MD simulations suggest the presence of $B^{[4]}$-O-$B^{[4]}$ linkages in borosilicate glasses. Indeed, the presence of the $B^{[4]}$-O-$B^{[4]}$ linkage was predicted by Gupta's random pair model[38] in the 1980s. Thus, it seems plausible that the $B^{[4]}(1B^{[4]},3Si^{[4]})$ units in N-BK7 observed in our MD simulations may correspond to the NMR results of $B_3^{[4]}$(-1.3 ppm) in this work.

The inset figures in Figure 3 show the ratios of $\frac{B_1^{[4]}}{B_3^{[4]}}$ for N-BK7 glass and $\frac{B_1^{[4]}}{B_2^{[4]}}$ for Boro33 glass. The MD simulations show a similar trend as the NMR results, i.e., both $\frac{B_1^{[4]}}{B_3^{[4]}}$ and $\frac{B_1^{[4]}}{B_2^{[4]}}$ increase with increasing pressure, despite the difference in absolute values. Representative atomic structures and the corresponding $B^{[4]}$ to $B^{[4]}$ conversion of three different $B^{[4]}$ species are also illustrated in Figure 1. However, we note that all the NNN predictions from MD simulations have high standard deviations.

Since oxygen is the atom with the highest concentration in N-BK7 (61% of 3073 atoms) and Boro33 (64 % 3073 atoms) in the MD simulation box, the oxygen species from the last statistically averaged configurations in the MD simulations have been analyzed to further quantify the atomic origin of volume densification in the borosilicate glasses. As shown in Figure 4, the oxygen species statistics show that $Si^{[4]}$-O-$Si^{[4]}$ and B-O-$Si^{[4]}$ share more than 90% of the total oxygen atoms. Among these, $Si^{[4]}$-O-$Si^{[4]}$ and $B^{[4]}$-O-$Si^{[4]}$ linkages consist of $23 \pm 1\%$ and $13 \pm 1\%$ of non-bridging oxygens (NBOs) in the second nearest neighbor silicon and boron tetrahedral networks in N-BK7 glass, respectively. In the Boro33 glass, the $Si^{[4]}$-O-$Si^{[4]}$, $B^{[3]}$-O-$Si^{[4]}$ and $B^{[4]}$-O-$Si^{[4]}$ linkages consist of $4 \pm 1\%$, $3 \pm 1\%$ and $2 \pm 1\%$ of NBOs in the second nearest neighbor including trigonal boron, tetrahedral silicon, and boron networks, respectively. All the oxygen species (including the second nearest neighbor NBOs) have the same total numbers, except for a slight change (<1 %/GPa) of B-O-$Si^{[4]}$ in both N-BK7 and Boro33 as a function of pressure.

The bond angle change of network formers, the bond length change of network modifiers, and the B or Al coordination change are considered as the primary mechanisms for volume densification in borosilicate glasses.[10, 13, 39, 40] To further explore the atomic origin, the average bond lengths and bond angles change have been calculated based on the last statistically averaged configurations in the MD simulations (see Table 3 and Table 4). The cutoffs for calculating all different bonds are reported in Table 3, which are based on the pair distribution functions[22]. The average bond lengths of Si-O, B-O, B-Si, and B-B remain the same regardless of the large molar volume change (~2 GPa), which is consistent with previous studies on SiO_2 and B_2O_3 glasses.[39, 41] The average bond length of Si-Si has a very small change (~0.015 Å/GPa). Moreover, the average bond lengths change of Na-O and K-O are around 0.01-0.02 Å/GPa, consistent with previous results[40, 42] on Na-O in sodium aluminosilicate glasses. Nevertheless, these bond lengths changes are not significant considering the standard deviation of the data.

As shown in Table 4, the O-Si-O and O-B-O bonds are the most frequent ones (≥75 %) in the glasses, and their average bond angles are independent of pressure (considering the uncertainty of the data sets). However, the bond angles of Si-O-Si, B-O-B, and B-O-Si are much more sensitive to the hot compression compared to the variations of average bond lengths. The bond angles of Si-O-Si and $B^{[4]}$-O-Si are slightly different among N-BK7 and Boro33 glasses, which is due to the different

applied interatomic potential functions as discussed in Ref. [20]. A bond angle decrease of 0.6°/GPa is observed for Si-O-Si and $B^{[4]}$-O-Si in N-BK7 glass, while one of 1°/GPa is observed in Boro33 glass. The change in bond angle of $B^{[3]}$-O-Si is less significant than that of $B^{[4]}$-O-Si considering the high standard deviation. The B-O-B bond angle also has a significant decrease upon densification, although it has a high uncertainty due to its the small population.

4. Discussion

We have found that Si-O-Si and $B^{[4]}$-O-Si have the same pressure-induced changes in bond angles in N-BK7 and Boro33 glasses, indicating similar strengths of the angular constraints of Si-O-Si and $B^{[4]}$-O-Si. Moreover, the bond angle changes of Si-O-Si and $B^{[4]}$-O-Si (total 24% at 2 GPa) in N-BK7 glass are 0.6°/GPa, which is smaller than that in Boro33 glass (1°/GPa with 19% of total Si-O-Si and $B^{[4]}$-O-Si). This is consistent with the early conclusion from Bridgman[39] that bond bending becomes more difficult when foreign atoms are embedded in the structure of soda silica glasses. Indeed, the present MD simulations have shown that N-BK7 glass has 6 times more second nearest neighbor NBOs in the Si-O-Si and $B^{[4]}$-O-Si linkages compared to Boro33.

Interestingly, we have found an approximate relation (see Figure 5) between the pressure-induced change in Si-O-Si and $B^{[4]}$-O-Si bond angle (ΔBA, GPa^{-1}), the total fraction (w) of Si-O-Si and $B^{[4]}$-O-Si linkages, and the pressure-induced molar volume change ($\Delta V_m/V_{m0}$, GPa^{-1}). Namely,

$$\frac{\Delta V_m}{V_{m0}} = \frac{\Delta BA}{w * C} \quad , \tag{3}$$

where ΔBA of N-BK7 is 0.6°/GPa and w equal to 0.24; ΔBA of Boro33 is 1°/GPa and w equal to 0.19; V_{m0} is the initial molar volume, C is a constant equal to 100°. The calculated values of $\Delta V_m/V_{m0}$ are in an excellent agreement with the experimental ones for N-BK7 (-0.6/24≈-2.5 %/GPa) and Boro33 (-1/19≈-5.0 %/GPa). Although the bond angles and bond lengths are in principle correlated with each other, various studies of densified silicate glasses have demonstrated how bond angles may change significantly while the bond lengths remain almost constant (due to the high standard deviation).[26, 39, 41, 43] It also has been reported that the reduction of the Si-O-Si bond angle decreases the distance of oxygen to second-nearest-neighbor to oxygen (O-O-O) and then decreases the molar volume.[43] However, the present MD simulations did not capture such distance change in O-O-O (Table 3) in

densified N-BK7 and Boro33 glasses. Therefore, we suggest a simple approach for quantifying the volume densification of N-BK7 and Boro33 glasses by considering the bond angle changes of Si-O-Si and $B^{[4]}$-O-Si following Eq. (3). We note that the presence of modifiers also influences the volume densification of N-BK7 and Boro33 glasses by increasing the difficulty of bond bending of Si-O-Si and $B^{[4]}$-O-Si and decreasing the bond lengths (~0.015 Å/GPa). In addition, the $B^{[3]}$ to $B^{[4]}$ conversion will increase the amount of $B^{[4]}$-O-Si linkages, and thus, decrease the molar volume of N-BK7 and Boro33.

The $B^{[4]}$ to $B^{[4]}$ conversion has been investigated by NMR in this study, showing that $B_3^{[4]}$ ($1B^{[4]},3Si^{[4]}$) and $B_2^{[4]}$($1B^{[3]},3Si^{[4]}$) are gradually transformed to $B_1^{[4]}$($0B,4Si^{[4]}$) with the increase of the quench pressure. The NNN analysis from the MD simulations, which is greatly influenced by very high standard deviations and oxygen tri-clusters, failed to capture the absolute amount of $B^{[4]}$ to $B^{[4]}$ conversion. One reason could be the orders of magnitude difference in cooling rates between hot compression experiments (2 K/min) and simulated pressure-quenching (5 K/ps). We also note that small amount (<5 %) of $B_2^{[4]}$($1B^{[3]},3Si^{[4]}$) is detected in N-BK7 glass, which will not influence the overall predictions by MD simulations. Nevertheless, the MD simulations qualitatively captured the increase of $\frac{B_1^{[4]}}{B_3^{[4]}}$ and $\frac{B_1^{[4]}}{B_2^{[4]}}$ with pressure. This is a new mechanism to explain the different pressure dependence of $B^{[4]}$ in densified N-BK7 and Boro33 glasses, which might answer the question why an early study[14] on pressurized borosilicate glass reported no detectable $B^{[3]}$ to $B^{[4]}$ conversion.

Finally, we note that the MD simulations based on Du's potential for N-BK7 glass have a linear frozen-in pressure inside the glass after the hot compression process, consistent with the previous experiments[19]. However, the MD simulations based on Bauchy's potential for Boro33 glass underestimated the frozen-in pressure after the hot compression process. Besides, we also note that the calculated average bond lengths of $B^{[3]}$-O (~1.39 Å) and $B^{[4]}$-O (~1.46 Å) for Boro33 (Bauchy's potential) is in agreement with the previous study[20], however, the ones for N-BK7 (Du's potential) is overall ~0.15 Å higher than Boro33. Moreover, all the MD simulations conducted in this work as well as other studies[20, 37] on borosilicate glass reported a very limited boroxol ring formation[37, 44, 45]. Thus, considering the above limitations from MD simulations as well as the comparison approach used in this work, the direct interpretation of the NMR data in terms of the MD models contains certain limitations.

5. Conclusion

In this study, we have quantitatively investigated the primary volume densification mechanisms of commercial N-BK7 and Boro33 glasses, which have been hot compressed up to 2 GPa above the glass transition temperature for 0.5 h and then annealed using a cooling rate of 2 K/min, via solid-state NMR and MD simulations. The results from density and ^{11}B MAS NMR measurements show that the molar volumes of N-BK7 and Boro33 decrease ~5% and ~10%, respectively, after the hot compression at 2 GPa, while the fraction $B^{[4]}$ increased ~13% in N-BK7 but only ~2% in Boro33 at 2 GPa. In addition, three different types of $B^{[4]}$ are detected from ^{11}B NMR, which can be confirmed in MD simulations as $B_1^{[4]}$(0B,4Si$^{[4]}$), $B_2^{[4]}$(1B$^{[3]}$,3Si$^{[4]}$) and $B_3^{[4]}$(1B$^{[4]}$,3Si$^{[4]}$). Moreover, the MD simulations can overall capture the $B^{[4]}$ populations as well as predict the pressure-induced change in $B^{[4]}$ fraction for Boro33 but underestimate that of N-BK7 (only ~6%) at 2 GPa. Furthermore, the reduction of molar volume is suggested to be a linear function of the bond angle change and fraction of Si-O-Si and $B^{[4]}$-O-Si. The modifiers and boron coordination conversion will also influence the volume densification of borosilicate glasses by increasing the difficulty of bond bending as well as decrease the bond lengths (~0.015 Å/GPa) and increase the $B^{[4]}$-O-Si populations, respectively. Lastly, the $B^{[4]}$ to $B^{[4]}$ conversion ($B_2^{[4]}$(1B$^{[3]}$,3Si$^{[4]}$) and $B_3^{[4]}$(1B$^{[4]}$,3Si$^{[4]}$) to $B_1^{[4]}$(0B,4Si$^{[4]}$)) has been observed in hot compressed N-BK7 and Boro33 glasses based on the NMR analysis and qualitatively confirmed by the MD simulations.

Acknowledgments

Linfeng Ding is funded by the Deutsche Forschungsgemeinschaft (DFG) as a DFG Fellowship (GZ: DI 2545). Kuo-Hao Lee is funded by SCHOTT AG, Mainz, Germany. The authors appreciate Dr. Clemens Kunisch (SCHOTT) providing glass samples and valuable comments. The authors thank the technicians and engineers at the SCHOTT machine shop for the sample preparation.

References

1. Varshneya AK, Mauro JC. Fundamentals of Inorganic Glasses. 3rd Edition. Amsterdam, Netherlands: Elsevier; 2019.

2. Kapoor S, Wondraczek L, Smedskjaer MM. Pressure-induced densification of oxide glasses at the glass transition. Frontiers in Materials. 2017;4:1.
3. Smedskjaer MM, Youngman RE, Striepe S, Potuzak M, Bauer U, Deubener J, et al. Irreversibility of Pressure Induced Boron Speciation Change in Glass. Sci Rep. 2014;4.
4. Lee SK, Mibe K, Fei Y, Cody GD, Mysen BO. Structure of B_2O_3 Glass at High Pressure: A B11 Solid-State NMR Study. Phys Rev Lett. 2005;94:165507.
5. Du L-S, Stebbins JF. Nature of silicon− boron mixing in sodium borosilicate glasses: a high-resolution 11B and 17O NMR study. The Journal of Physical Chemistry B. 2003;107:10063-76.
6. Sen S, Topping T, Yu P, Youngman R. Atomic-scale understanding of structural relaxation in simple and complex borosilicate glasses. Physical Review B. 2007;75:094203.
7. Edwards T, Endo T, Walton JH, Sen S. Observation of the transition state for pressure-induced $BO_3 \rightarrow BO_4$ conversion in glass. Science. 2014;345:1027-29.
8. Østergaard MB, Youngman RE, Svenson MN, Rzoska SJ, Bockowski M, Jensen LR, et al. Temperature-dependent densification of sodium borosilicate glass. RSC Advances. 2015;5:78845-51.
9. Wondraczek L, Sen S, Behrens H, Youngman RE. Structure-energy map of alkali borosilicate glasses: Effects of pressure and temperature. Physical review B. 2007;76:014202.
10. Wu J, Gross TM, Huang L, Jaccani SP, Youngman RE, Rzoska SJ, et al. Composition and pressure effects on the structure, elastic properties and hardness of aluminoborosilicate glass. J Non-Cryst Solids. 2020;530:119797.
11. Bista S, Stebbins JF, Wu J, Gross TM. Structural changes in calcium aluminoborosilicate glasses recovered from pressures of 1.5 to 3GPa: Interactions of two network species with coordination number increases. J Non-Cryst Solids. 2017;478:50-57.
12. Wondraczek L, Behrens H, Yue YZ, Deubener J, Scherer GW. Relaxation and glass transition in an isostatically compressed diopside glass. J Am Ceram Soc. 2007;90:1556-61.
13. Svenson MN, Youngman RE, Yue Y, Rzoska SJ, Bockowski M, Jensen LR, et al. Volume and structural relaxation in compressed sodium borate glass. Physical Chemistry Chemical Physics. 2016;18:29879-91.

14. Du L-S, Allwardt J, Schmidt B, Stebbins J. Pressure-induced structural changes in a borosilicate glass-forming liquid: boron coordination, non-bridging oxygens, and network ordering. J Non-Cryst Solids. 2004;337:196-200.
15. Stevensson B, Yu Y, Edén M. Structure–composition trends in multicomponent borosilicate-based glasses deduced from molecular dynamics simulations with improved B–O and P–O force fields. Physical Chemistry Chemical Physics. 2018;20:8192-209.
16. Wang MY, Krishnan NMA, Wang B, Smedskjaer MM, Mauro JC, Bauchy M. A new transferable interatomic potential for molecular dynamics simulations of borosilicate glasses. J Non-Cryst Solids. 2018;498:294-304.
17. Deng L, Du JC. Development of boron oxide potentials for computer simulations of multicomponent oxide glasses. J Am Ceram Soc. 2019;102:2482-505.
18. Sundararaman S, Huang L, Ispas S, Kob W. New interaction potentials for borate glasses with mixed network formers. The Journal of chemical physics. 2020;152:104501.
19. Ding L, Buhre S, Kunisch C, Kaus B. Pressure dependence of density and structural relaxation of glass near the glass transition region. J Am Ceram Soc. 2018;101:1149-58.
20. Fortino M, Berselli A, Stone-Weiss N, Deng L, Goel A, Du J, et al. Assessment of interatomic parameters for the reproduction of borosilicate glass structures via DFT-GIPAW calculations. J Am Ceram Soc. 2019;102:7225-43.
21. Wang M, Krishnan NA, Wang B, Smedskjaer MM, Mauro JC, Bauchy M. A new transferable interatomic potential for molecular dynamics simulations of borosilicate glasses. J Non-Cryst Solids. 2018;498:294-304.
22. Lee K-H, Yang Y, Ziebarth B, Mannstadt W, Davis MJ, Mauro JC. Evaluation of classical interatomic potentials for molecular dynamics simulations of borosilicate glasses. J Non-Cryst Solids. 2020;528:119736.
23. Boffy R, Peuget S, Schweins R, Beaucour J, Bermejo FJ. High thermal neutron flux effects on structural and macroscopic properties of alkali-borosilicate glasses used as neutron guide substrate. Nuclear Instruments and Methods in Physics Research Section B: Beam Interactions with Materials and Atoms. 2016;374:14-19.

24. Dell W, Bray P, Xiao S. ^{11}B NMR studies and structural modeling of Na_2O-B_2O_3-SiO_2 glasses of high soda content. J Non-Cryst Solids. 1983;58:1-16.
25. Plimpton S. Fast Parallel Algorithms for Short-Range Molecular Dynamics. Journal of Computational Physics. 1995;117:1-19.
26. Bauchy M. Structural, vibrational, and thermal properties of densified silicates: Insights from molecular dynamics. J Chem Phys. 2012;137.
27. Ossendrijver M. Ancient Babylonian astronomers calculated Jupiter's position from the area under a time-velocity graph. Science. 2016;351:482-84.
28. Massiot D, Fayon F, Capron M, King I, Le Calvé S, Alonso B, et al. Modelling one-and two-dimensional solid-state NMR spectra. Magn Reson Chem. 2002;40:70-76.
29. Youngman R, Zwanziger J. Multiple boron sites in borate glass detected with dynamic angle spinning nuclear magnetic resonance. J Non-Cryst Solids. 1994;168:293-97.
30. Prasad S, Clark TM, Sefzik TH, Kwak H-T, Gan Z, Grandinetti PJ. Solid-state multinuclear magnetic resonance investigation of Pyrex®. J Non-Cryst Solids. 2006;352:2834-40.
31. Wu J, Stebbins JF. Quench rate and temperature effects on boron coordination in aluminoborosilicate melts. J Non-Cryst Solids. 2010;356:2097-108.
32. Howes A, Vedishcheva N, Samoson A, Hanna J, Smith M, Holland D, et al. Boron environments in Pyrex® glass—a high resolution, Double-Rotation NMR and thermodynamic modelling study. Physical Chemistry Chemical Physics. 2011;13:11919-28.
33. Tricot G. The structure of Pyrex® glass investigated by correlation NMR spectroscopy. Physical Chemistry Chemical Physics. 2016;18:26764-70.
34. Lee SK, Stebbins JF. Al–O–Al and Si–O–Si sites in framework aluminosilicate glasses with Si/Al= 1: quantification of framework disorder. J Non-Cryst Solids. 2000;270:260-64.
35. Lee S, Stebbins J. Extent of intermixing among framework units in silicate glasses and melts. Geochimica et Cosmochimica Acta. 2002;66:303-09.
36. Yu Y, Stevensson B, Edén M. Medium-range structural organization of phosphorus-bearing borosilicate glasses revealed by advanced solid-state NMR experiments and MD simulations: consequences of B/Si substitutions. The Journal of Physical Chemistry B. 2017;121:9737-52.

37. Yu Y, Stevensson B, Edén M. Direct Experimental Evidence for Abundant BO_4–BO_4 Motifs in Borosilicate Glasses from Double-Quantum ^{11}B NMR Spectroscopy. The journal of physical chemistry letters. 2018;9:6372-76.
38. Gupta PK, "Random-pair model of four-coordinated borons in alkali-borate glasses," in International Congress on Glass, Collected Papers, 14 th. Vol. 11.
39. Bridgman PW, Simon I. Effects of Very High Pressures on Glass. Journal of Applied Physics. 1953;24:405-13.
40. Kelsey KE, Stebbins JF, Mosenfelder JL, Asimow PD. Simultaneous aluminum, silicon, and sodium coordination changes in 6 GPa sodium aluminosilicate glasses. American Mineralogist. 2009;94:1205-15.
41. Trease NM, Clark TM, Grandinetti PJ, Stebbins JF, Sen S. Bond length-bond angle correlation in densified silica—Results from ^{17}O NMR spectroscopy. The Journal of Chemical Physics. 2017;146:184505.
42. Lee SK, Cody GD, Fei Y, Mysen BO. The effect of Na/Si on the structure of sodium silicate and aluminosilicate glasses quenched from melts at high pressure: A multi-nuclear (Al-27, Na-23, O-17) 1D and 2D solid-state NMR study. Chemical Geology. 2006;229:162-72.
43. Devine R, Dupree R, Farnan I, Capponi J. Pressure-induced bond-angle variation in amorphous SiO_2. Physical Review B. 1987;35:2560.
44. Maranas JK, Chen Y, Stillinger DK, Stillinger FH. Polarization interactions and boroxol ring formation in boron oxide: A molecular dynamics study. The Journal of Chemical Physics. 2001;115:6578-89.
45. Scherer C, Schmid F, Letz M, Horbach J. Structure and dynamics of B_2O_3 melts and glasses: From ab initio to classical molecular dynamics simulations. Computational Materials Science. 2019;159:73-85.

Table captions

Table 1 Compositions and properties of N-BK7 and Boro33 provide by SCHOTT AG.

Table 2 Experimental conditions and results of boron species from NMR and MD simulations.

Table 3 Average bond lengths in the borosilicate glasses as calculated from the MD simulations.

Table 4 Average bond angles in the borosilicate glasses as calculated from the MD simulations.

Figure captions

Figure 1 ^{11}B MAS NMR spectra of (a) N-BK7 glass and (b) Boro33 glass at various pressure and temperature conditions. All the samples were annealed at a cooling rate of 2 K/min. The inset in (a) on the left side shows the zoomed-in spectra of the $B^{[3]}$. The blue dash lines are the deconvolutions of 1atm sample. From high to low frequencies, these deconvolutions represent $B^{[3]}$ ring (17.3 ± 0.1 ppm), $B^{[3]}$ nonring (13.3 ± 0.1 ppm), (a) $B_3^{[4]}(1B^{[4]},3Si^{[4]})$ (-1.3 ± 0.1 ppm), (b) $B_2^{[4]}(1B^{[3]},3Si^{[4]})$ (-0.2 ± 0.1 ppm), $B_1^{[4]}(0B,4Si^{[4]})$ (-2 ± 0.3 ppm). The schematic atomic structure on the right side is from the MD simulations, in which the light yellow atom represents B, the blue atom represents Si, the red atom represents O, and the yellow atom represents Na or K.

Figure 2 Pressure dependence of molar volume (circles) and $B^{[4]}$ (from NMR, triangles) of (a) N-BK7 and (b) Boro33 glasses. The arrows of dashed lines represent the overall trend of the data (not the mathematically computed one).

Figure 3 The fractions of next nearest neighbors (NNNs) of $B^{[4]}$ in different densified (a) N-BK7 and (b) Boro33 glasses as calculated from MD simulations. $B^{[4]}(O^{[3]})$ consists of all different NNN containing O tri-clusters. $B_1^{[4]}$=$B^{[4]}(0B,4Si^{[4]})$, $B_2^{[4]}$= $B^{[4]}(1B^{[3]},3Si^{[4]})$ and $B_3^{[4]}$= $B^{[4]}(1B^{[4]},3Si^{[4]})$. Error bars represent the standard deviation of five MD simulations.

Figure 4 Oxygen species of different densified (a) N-BK7 and (b) Boro33 glasses in the MD simulations. All the oxygen species includes bridging and non-bridging oxygens in the second nearest neighbor networks. The amount of NBOs has no change as a function of pressure. Error bars represent the standard deviation of five MD simulations.

Figure 5 Approximate relation between the pressure-induced change in Si-O-Si and $B^{[4]}$-O-Si bond angle (ΔBA) and the total fraction (w) of Si-O-Si and $B^{[4]}$-O-Si linkages compared to the pressure-

induced molar volume change ($\Delta V_m/V_{m0}$) of N-BK7 and Boro33 glasses. C is a constant and error bars are estimated from the standard deviations of ΔBA.

Table 1 Compositions and properties of N-BK7 and Boro33 provide by SCHOTT AG.

Glass ID	SiO_2 [mol %]	B_2O_3 [mol %]	Na_2O [mol %]	K_2O [mol %]	Al_2O_3 [mol %]	$T_{g,vis}$ [℃]	Poisson's ratio	Density [g/cm^3]
N-BK7*	74.5	10.2	10.2	5.1	0	561	0.20	2.51
Boro33	83.7	11.1	3.3	0.4	1.5	560	0.21	2.23

* N-BK7 glass also contains very small amounts of CaO and BaO. We simplified here for the convenience of MD simulations.

Table 2 Experimental conditions and results of boron species from NMR and MD simulations.

Sample ID	Experimental conditions	$B^{[3]}$ ring* [%]	$B^{[3]}$ nonring§ [%]	$B_1^{[4]}$ (0B,4Si[4]) [%]	$B_2^{[4]}$ (1B[3],3Si[4]) [%]	$B_3^{[4]}$ (1B[4],3Si[4]) [%]	$B^{[4]}$ ratio¶	$B^{[4]}_{total}$ (±2†) [%]	$B^{[4]}_{MD}$ (±2‡) [%]
N-BK7									
N1	1atm-560℃ /4h	6.4	7.6	35.2	-	50.8	0.69	86	89 (V_m=7.86 cm^3/mol)
N2	1GPa-560℃ /0.5h	2.5	3.1	47.1	-	47.3	1.00	94.4	
N3	1GPa-580℃ /0.5h	1.9	3.1	46.9	-	48.1	0.98	95	92 (V_m=7.66 cm^3/mol)
N4	1GPa-600℃ /0.5h	1.4	2.4	47.4	-	48.8	0.97	96.2	
N5	2GPa-580℃ /0.5h	1.3	1.1	48.9	-	48.7	1.01	97.7	
N6	2GPa-600℃ /0.5h	0.9	1	54.5	-	43.6	1.25	98.1	95 (V_m=7.46 cm^3/mol)
N7	2GPa-700℃ /0.5h	0.3	0.7	62.4	-	36.6	1.70	99.0	
Boro33									
B1	1atm-560℃ /4h	46.5	32.2	6.5	14.8	-	0.44	21.3	18 (V_m=8.64 cm^3/mol)
B2	1GPa-560℃ /0.5h	54	24.9	10.7	10.4	-	1.03	21.1	
B3	1GPa-580℃ /0.5h	56.5	21.9	11.8	9.8	-	1.20	21.6	19 (V_m=8.18 cm^3/mol)
B4	1GPa-600℃ /0.5h	56.8	21.9	11.9	9.4	-	1.27	21.3	
B5	2GPa-580℃ /0.5h	59.9	17.1	15.8	7.2	-	2.19	23	
B6	2GPa-600℃ /0.5h	59.9	17.5	15.9	6.6	-	2.41	22.5	20 (V_m=7.80 cm^3/mol)
B7	2GPa-700℃	61.5	16.1	16.6	5.8	-	2.86	22.4	

/0.5h

* ^{11}B NMR parameters obtained from *Dmfit*: δ_{iso}=17.3±0.1 ppm, C_Q=2.64±0.01 MHz, η_Q=0.30±0.01

§ ^{11}B NMR parameters obtained from *Dmfit*: δ_{iso}=13.3±0.1 ppm, C_Q=2.66±0.01 MHz, η_Q=0.26±0.01

¶ $B^{[4]}$ ratio is $\frac{B_1^{[4]}}{B_3^{[4]}}$ for N-BK7 glass and $\frac{B_1^{[4]}}{B_2^{[4]}}$ for Boro33 glass

† ^{11}B NMR deconvolution error for fraction is 2 %

‡ Standard deviation from five simulations

Table 3 Average bond lengths in the borosilicate glasses as calculated from the MD simulations.

Glass	V_m [cm³/mol]	Si-O [Å]	$B^{[3]}$-O [Å]	$B^{[4]}$-O [Å]	Si-Si [Å]	B-Si [Å]	B-B [Å]	Na-O [Å]	K-O [Å]	Al-O [Å]	B-Al [Å]	O-O-O* [Å]
N-BK7 (Du's potential)	Cutoff [Å]	2	2	2	3.5	3.5	3.4	3	4	-	-	3.5-6
	7.86	1.61±0.00	1.54±0.00	1.60±0.00	3.11±0.00	3.04±0.00	2.94±0.02	2.58±0.01	2.93±0.03	-	-	4.81±0.00
	7.66	1.61±0.00	1.54±0.01	1.60±0.01	3.10±0.01	3.03±0.00	2.94±0.01	2.56±0.01	2.90±0.01	-	-	4.81±0.00
	7.46	1.61±0.00	1.54±0.01	1.59±0.01	3.09±0.01	3.02±0.00	2.94±0.05	2.54±0.01	2.87±0.02	-	-	4.81±0.00
Boro33 (Bauchy's potential)	Cutoff [Å]	2	1.8	1.8	3.5	3.2	3	3	4	2.2	3.5	3.5-6
	8.64	1.64±0.00	1.39±0.00	1.46±0.00	3.13±0.01	2.90±0.01	2.76±0.01	2.65±0.01	3.43±0.03	1.77±0.00	2.83±0.05	4.82±0.00
	8.18	1.64±0.00	1.39±0.00	1.46±0.00	3.12±0.00	2.89±0.01	2.77±0.01	2.64±0.02	3.42±0.03	1.77±0.00	2.88±0.03	4.82±0.00
	7.80	1.64±0.00	1.39±0.00	1.46±0.00	3.11±0.00	2.90±0.00	2.75±0.01	2.63±0.01	3.37±0.03	1.76±0.01	2.87±0.03	4.82±0.00

* Oxygen-second-nearest-neighbor-oxygen

Table 4 Average bond angles in the borosilicate glasses as calculated from the MD simulations.

Glass	V_m [cm^3/mol]	O-Si-O (60 %*)	O-B-O (16 %)	Si-O-Si (15 %)	B-O-B (1 %)	$B^{[3]}$-O-Si	$B^{[4]}$-O-Si
N-BK7 (Du's potential)	7.86	109.4±0.0°	110.0±0.1°	151.0±0.4°	140.1±1.1°	150.0±1.7° (1 %)	145.8±0.4° (8 %)
	7.66	109.4±0.0°	109.8±0.1°	150.7±0.2°	138.9±1.8°	149.6±3.7° (1 %)	145.0±0.4° (8 %)
	7.46	109.3±0.0°	109.8±0.1°	149.7±0.4°	135.6±1.6°	148.6±3.3° (0 %)	144.6±0.2° (9 %)
Glass	Pressure	O-Si-O (65 %)	O-B-O (10 %)	Si-O-Si (17 %)	B-O-B (0 %)	$B^{[3]}$-O-Si (6 %)	$B^{[4]}$-O-Si (2 %)
Boro33 (Bauchy's potential)	8.64	109.4±0.0°	116.9±0.3°	148.8±0.3°	155.2±3.2°	148.2±0.4°	143.2±1.1°
	8.18	109.3±0.0°	116.6±0.2°	147.8±0.5°	156.3±2.4°	147.8±0.6°	142.2±1.6°
	7.80	109.3±0.0°	116.0±0.3°	146.8±0.2°	151.7±2.3°	147.6±0.2°	141.2±0.4°

* Each bond account for the percentages of total bonds in glass

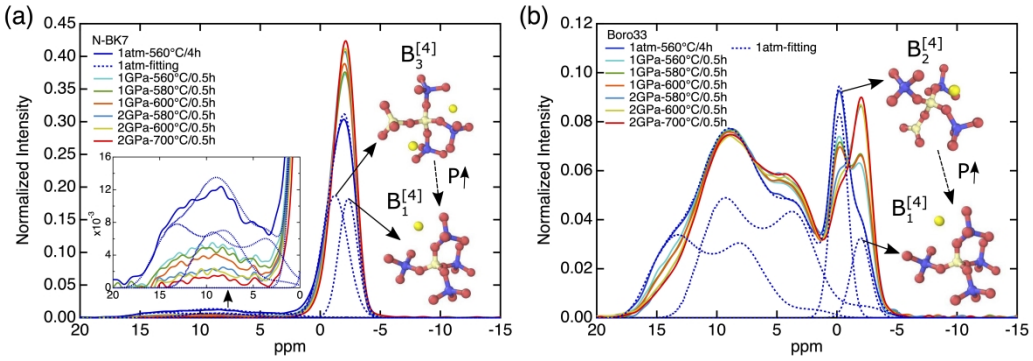

jace_17377_f1.jpg

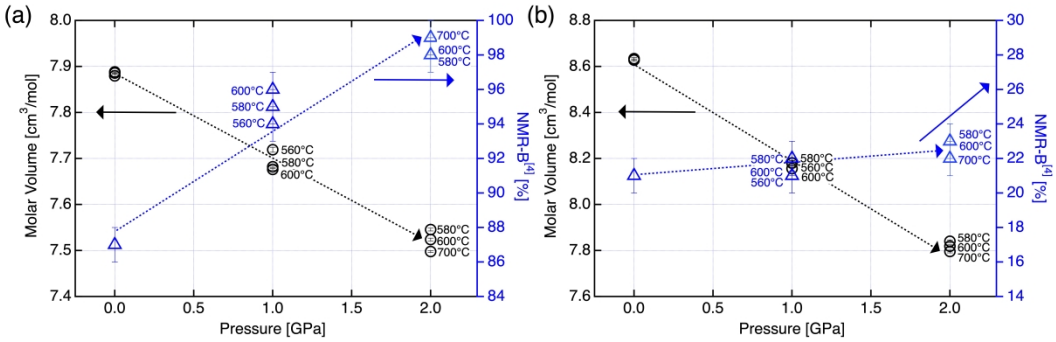

jace_17377_f2.jpg

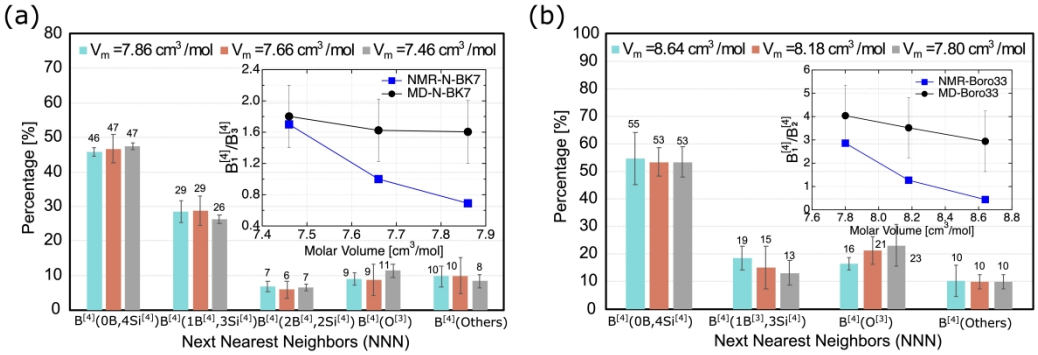

jace_17377_f3.jpg

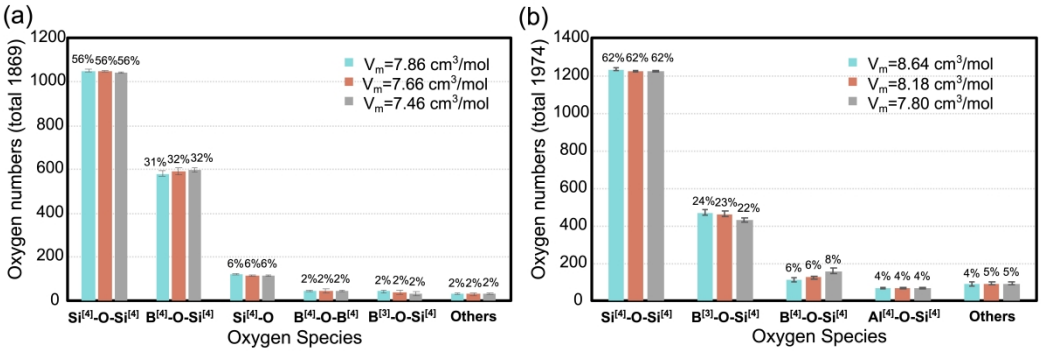

jace_17377_f4.jpg

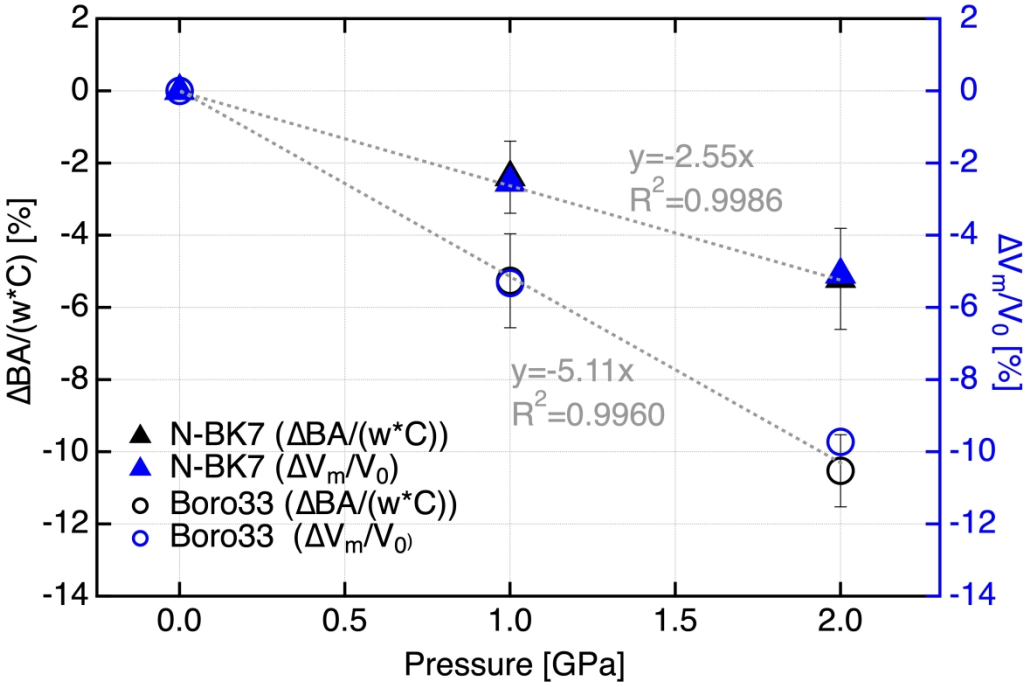

jace_17377_f5.jpg